Journal de Mécanique,
Vol. 16, N° 5, 1977.

Theory and experiments on plane shear flow instabilities in nematics*

by

E. DUBOIS-VIOLETTE**, E. GUYON**,
I. JANOSSY**, ***, P. PIERANSKI** and P. MANNEVILLE****

ABSTRACT. — A planar nematic (MBBA) sheared between parallel plates (perpendicular to z) with a velocity $v_y(z)$ perpendicular to the director $\mathbf{n}$ along x can undergo homogeneous or roll instabilities. This work discusses extensively both regimes in the case of continuous as well as alternating shear. Theoretical emphasis is put on simplified description (thresholds and wavelengths of rolls) dealing in particular with limiting behavior (large magnetic fields or shear frequencies) and extending a detailed theoretical analysis by E. Dubois-Violette and P. Manneville. The experiments are done in direct comparison with this description and develop the previous work of E. Guyon and P. Pieranski. They show that the high frequency behavior is characterized by a minimum displacement rather than shear. They also analyze the role of a high frequency (stabilizing) as well as low frequency (destabilizing) electric field E_z. The diffraction pattern produced by shining a parallel laser beam on the roll is used to characterize the behavior above threshold.

RÉSUMÉ. — Dans un nématique initialement orienté dans une direction (Ox), deux types d'instabilités, homogènes ou en rouleaux, apparaissent quand on applique un cisaillement [vitesse $v_y(z)$] entre deux plaques parallèles (à xOy).

Nous discutons ces deux régimes dans le cas d'un cisaillement continu et celui d'un cisaillement alternatif.

Une description théorique simplifiée est développée, notamment on étudie le comportement en champ magnétique élevé et à fréquence élevée. Cette description simplifiée repose sur l'analyse théorique faite par E. Dubois-Violette et P. Manneville. Les expériences précisent une description déjà donnée par P. Pieranski et E. Guyon.

* Supported in part by an Action Thématique Programmée of C.N.R.S.; this article covers part of the thesis of P. Pieranski and P. Manneville.

** Laboratoire de Physique des Solides, associé au C.N.R.S., Université Paris-Sud, Centre d'Orsay, 91405 Orsay, France.

*** On leave from Central Research Institute for Physics, Budapest, Hungary.

**** Service de Physique du Solide et de Résonance Magnétique, Centre d'Études nucléaires de Saclay, B.P. n° 2, 91190 Gif-sur-Yvette, France.

Nous montrons que le comportement à haute fréquence est caractérisé par un déplacement minimum des plaques. L'influence d'un champ électrique E_z est analysée : rôle stabilisant à haute fréquence et déstabilisant à basse fréquence. Le comportement au-dessus du seuil est étudié à l'aide de la figure de diffraction, en lumière parallèle, d'un faisceau laser.

1. Introduction

Over the last years we have investigated systematically some hydrodynamic instabilities in well aligned nematic liquid crystals. A first study ([1], I in the following) dealt with the effect of a simple plane shear, $s = \partial v_y/\partial z$ = constant, applied on a nematic aligned along x (see *Fig.* 1).

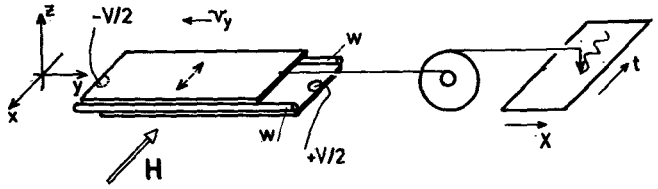

Fig. 1. — Schematic of the cell indicating the director alignment (←——→) between two parallel plates. An alternating voltage V (F) and a magnetic field H can be applied. The motion of the upper plate defined by spacer wires (w) is obtained from the X motion of a X t recorder.

Two types of instabilities were obtained: an *homogeneous* one [2] (H in the following) with a distortion uniform across xy planes parallel to the limiting plates, and a mode involving a periodic distortion of the director with a formation of *rolls* with axis along the flow direction (R mode). These effects were understood as coming from a balance between destabilizing hydrodynamic torques described by the Ericksen-Leslie-Parodi (E. L. P.) stress tensor and the stabilizing elastic torques. The effect of magnetic and electric torques coming from applied fields (E_z along z, H_x along x) was also studied. The discussion of the roll formation was carried as an extension of a description of the electrohydrodynamic instabilities in liquid crystals. More recently, two of us ([3], II in the following) have done a detailed analytical and numerical study of the same shear flow problem both in the H and R case. Our analysis of the H mode is fully consistent with an independent analytical approach by Leslie [4].

This theoretical interest has led us to the more detailed study presented in the present paper. The original features described here are: a study

of the flow pattern leading in particular to the observation of transverse flows in the H case, as had been predicted theoretically; a quantitative description of the cross-over between H and R regime in the presence of a field H_x; a more accurate characterization of the nature of the instability thresholds; a more complete description of the threshold curve for alternating flows. The alternating electric field E_z is used to stabilize or to destabilize the initial alignment and, consequently, to modify the thresholds.

The theoretical description develops that of reference [3]. We also present here a simplified analysis of the rolls which emphasizes the physical aspect of the problem and leads to an analytical description of some asymptotic behaviors both in the case of continuous and alternating flows: limit of high magnetic fields and, in the latter case, limit of high shear frequencies.

The situation discussed here displays certain analogies with the case of a Poiseuille flow between parallel plates, studied recently in detail experimentally [5] and theoretically [6]. It is however a simpler case than the Poiseuille problem and will be more appropriate for further extended studies of convective instabilities in nematics, including the behavior above threshold.

2. Experimental

Throughout the experiments, we have used methoxy-*p-n* benzilidene butyl anilin (MBBA) in its nematic phase at 25°C. The nematic state consists of a nearly parallel arrangment of these elongated rod like molecules; the local ordering is characterized by a unit vector $\mathbf{n}$, the director, aligned along the average molecular direction ($+\mathbf{n}$ is equivalent to $-\mathbf{n}$). It also gives the optical axis of this uniaxial material. In the present experiments a uniform initial alignment is obtained by a treatment of the limiting surfaces of the liquid crystal cell.

2.1. Plane geometry

In most experiments, we have used a shear flow cell similar to that described in I (*Fig.* 1). Two parallel plates (3×10 cm) perpendicular to z, separated by a distance $d \sim 100$ to 300 μ, are allowed to slide parallel to each other. The spacing is defined by parallel wires stretched along the length of the flow. The wires also prevent the existence of a net flow across the transverse direction. In another set-up the variable spacing

was adjusted by three teflon screws passing through the upper plate and making the contact with the lower one. The parallelism is easily verified by observing the Perot Fabry rings in parallel monochromatic light; their spacing leads to an accurate thickness measurement.

In the present experiments, the motion of the upper plate with respect to the fixed lower one is obtained by coupling it, through a system of reducing gears, to the displacement along X of an (X, t) recorder. This method permits us to produce various types of displacements to the cell, by injecting on the X axis a desired signal coming from a function generator, as well as to record the displacement of the upper plate. Continuous flows are obtained by applying a symmetric triangular signal of large enough amplitude, (amplitude of displacement of the upper plate, D up to 1 cm).

The planar alignment of the liquid crystal on the glass plates ($\mathbf{n}$ parallel to the x direction in the plane of the plates when no shear is applied) is obtained from oblique evaporation of a semi transparent conducting Au film. The conducting electrodes are also used to produce an electric field E_z across the cell. The orientation is characterized in the H case by the conoscopic image in converging monochromatic light. The rotation and tilt of the image are connected with the "twist" and "splay" components of the distortion (respectively n_y and n_z components of the director).

In the R case the formation of rolls is easily detected optically thanks to the large birefringence of nematics. An optical diffraction study of this mode is also possible and is discussed in *d*).

2.2. Cylindrical geometry

Near thresholds where long time constants are involved, the use of a saw-tooth signal of large amplitude to produce a "quasi d. c. flow" is not correct and the effective threshold is increased due to the alternating character of the shear.

A more appropriate experiment uses a cylindrical geometry (*Fig.* 2). In a lucite block, a cylindrical hole of $D_0 = 4$ mm diameter has been drilled. Within this hole, a tightly fitted lucite cylinder can be set into rotation. Over a third of its length, its diameter has been reduced to $D_i = 3.4$ mm thus creating an annular space in which a Couette flow is produced.

The initial director alignment ($\mathbf{n}$ along the cylinder axis x and perpendicular to the shear as in case *a*) is induced by rubbing the cylinders along the x direction prior to the filling of the cell.

A possible optical detection of the homogeneous distortion uses the reflection of an incident beam on a reflecting inner cylinder. A convergent monochromatic beam with an average oblique incidence is focused on the cell and the twist of the reflected conoscopic image is measured. We have tested this technique in independent test experiments using a planar geometry and a twist cell. However it is not appropriate in our cylinder

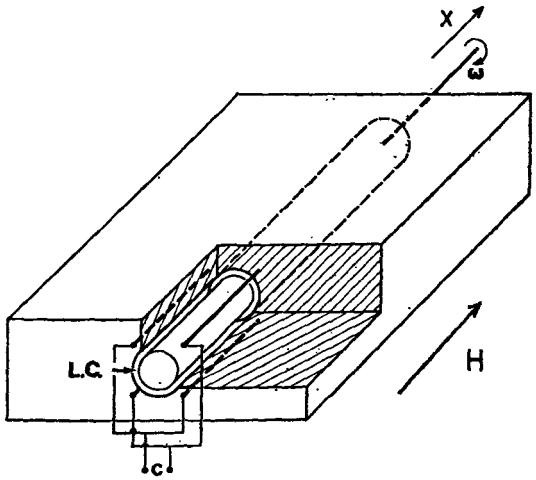

Fig. 2. — Cylindrical geometry. The liquid crystal (L. C.) is aligned parallel to the axis of rotation by polishing the inner and outer lucite cylinders. A quadrupolar arrangment is used to record the twist distortion.

with a small radius of curvature because of lens effects. A quadrupolar (see *Fig.* 2) technique has been used instead. The capacitance C of a system of 4 parallel wires connected 2 by 2 was measured as a function of the shear rate. The variation of the effective dielectric constant component along the azimuthal axis gives the amount of twist in the distortion. The total capacitance is very small ($\sim$ 1 pf) and the relative changes are weak ($\sim$ 1/100) due to the relatively small dielectric constant anisotropy of MBBA ($\varepsilon_a = \varepsilon_{||} - \varepsilon_{\perp} \sim -0.5$). An a. c. technique was used to characterize the variation of the capacitance above threshold.

Effect of the rotation on threshold

Two kinds of forces must be taken into account:

— the centrifugal one responsible for the classical Taylor instability;

– the anisotropic Leslie-Ericksen forces plus a coupling between both effects. To determine the exact nature of the instability, one needs to evaluate this coupling.

A first analysis was presented in [9] and we summarize here the relevant results of a more recent study [7].

In the case of the homogeneous mode considered here, the coupling is absent. The threshold of the homogeneous instability is not modified by the rotation.

The situation is different for the roll instability. The coupling depends on the average rotation ω_m and the relative variation of the critical shear rate s_c due to ω_m is of the order of $\omega_m (\rho d^2/\eta)$ where ρ is the density and η a typical viscosity. However instabilities, specific of nematics, correspond to very low thresholds. When one of the cylinders is at rest, as it is the case here, this implies ω_m very small and corrections due to rotation are completely negligible.

We may also mention, to conclude this discussion, the experiments by Cladis and Torza [8] in the Couette flow geometry with a different initial alignment and a different nematic where the usual Taylor threshold was observed for rotation rates much above the roll pattern associated with the R instability.

2.3. Visualization

The hydrodynamic motion is followed from the microscopic observation of the motion of dust particules or of articificially introduced small (2 μ) Cu grains. The cylindrical geometry with an horizontal axis is rather convenient as the small particles are continously recycled in the main flow in a vertical plane. We have observed that, in the homogeneous mode above threshold, the flow is deflected from the initial axial direction as predicted theoretically. We have also observed, in agreement with the theoretical predictions of references [4] and II, that the additional – transverse – component of the flow along the rotation axis x, $v_x(r)$, changes sign as one gets across the width of the cell. Rather amusingly, the grains which happen to be elongated align towards the direction of the distortion giving a relatively direct qualitative picture of the distortion.

The convective motion associated with the R instability has also been detected and is consistent with the flow pattern presented in II (see *Fig.* 12 of II).

2.4. Optical diffraction study of the roll instability

The threshold of the R instability as well as the characteristics above threshold (wavelength of the rolls, amplitude of the distortion) can be analyzed from the diffraction image given by a narrow parallel laser beam incident on the cell. The technique has already been described in the case of electrohydrodynamic instabilities in nematics in references [10] to [12] and we will give in a separate work a more detailed discussion of its application in the case of the present hydrodynamic ones [13]. A photocell having a linear response in intensity (Photodiode Pin 10 DP, united detector) is placed at the position of the most intense diffracted spot. The extrapolation to zero of the diffracted intensity gives a precise determination of the threshold. In the present experiments with a large (compared with the wavelength of light) wavelength of the rolls the diffraction pattern is due essentially to the phase grating produced by the periodic distortion of the director axis. Only the vertical component n_z is acting if the light beam is perpendicular to the shear flow cell. From the quantitative analysis of the intensity variation of the central as well as diffracted spot as a function of shear we have been able to obtain the variation of n_z just above the instability threshold.

The wavelength of the rolls is measured from the angle between consecutive diffraction rays. The n_y variation can be determined using a laser beam incident obliquely on the cell.

2.5. Application of a magnetic or electric field

Through the experiment, the magnetic field as well as the electric one are used to control the instability regimes. A magnetic field up to 10 kG produced by an electromagnet is applied parallel to the unperturbed director in plane and cylindrical geometries. The magnetic field parallel to the director is stabilizing and shortens the relaxation time of the director to the unperturbed state. It leads to increased thresholds and can reinforce the stabilizing action of elasticity if it is large enough. The alternating electric field E (F) can be applied across the cell using the evaporated Au films as electrods. A high frequency electric field E_z limits the distortion of the director out of the plane xy and decreases the relaxation time constant of the component n_z. We will see that this has a rather complex effect on the R threshold. A low frequency electric fiel of low intensity has a quite opposite effect. It tends to induce a convective electrohydrodynamic instability [14] and, by doing so, it increases the relaxation time constant of n_z.

3. Continuous shear

The mechanisms of the H and R instabilities have been largely described in [1], [2] and [3] and we send the reader to these references for a detailed presentation. The notations are the same as those of reference II. The case of the H instability is sketched on Figure 3 and involves a coupling

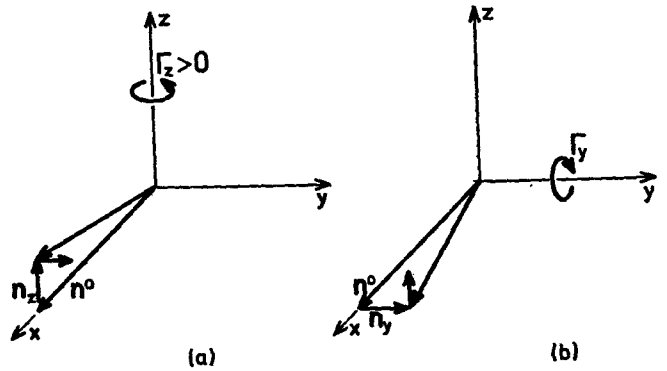

Fig. 3. — Mechanism for a homogeneous distortion. (*a*) Suppose a fluctuation $n_z > 0$. The flow induces a viscous torque $\Gamma_z > 0$ such that a fluctuation $n_y > 0$ appears. (*b*) Suppose a fluctuation $n_y > 0$. The flow induces a viscous torque Γ_y such that the initial fluctuation n_z is increased ($\alpha_3 < 0$).

between the n_y and n_z components of the distortion *via* the shear which causes viscous torques on these components. In the R case new force terms arise from the Leslie Ericksen Parodi stress tensor due to the variation of $\mathbf{n}$ along x. The equations describing the linear coupling between the n_y and n_z variables will be presented later [equations (3) to (4)].

3.1. Homogeneous instability

The homogeneous distortion mode, obtained with the director configuration indicated in Figure 1, involves both twist and splay; the interplay between the viscous torque components is constructive when the product of the two viscous torque coefficients α_2 and α_3 [15], $\alpha_2\,\alpha_3$, is positive (1).

(1) The torque coefficient α_2 ($|\alpha_2| > |\alpha_3|$ in general), measured in shear flow experiments when the director is initially perpendicular to the plates, is always negative. Both signs of α_3 can be obtained. A simple way to characterize $\alpha_3 < 0$ materials is to observe that for large enough shears the director aligns nearly along the flow axis. Also, if one uses a planar sample, aligned along a shear produced by moving an upper plate, one sees easily that the conoscopic image formed above the plate is first displaced "along" the direction of the shear when $\alpha_3 > 0$, "against" it when $\alpha_3 < 0$.

The product $-\alpha_2 sn_z$ [resp. $(\alpha_3 \eta_3/\eta_1) sn_y$] is the viscous torque experienced by $\mathbf{n}$ which tends to create a component n_y (resp n_z) parallel to y (resp. to z [3], [4]). In this work, we restrict our study to experiments on MBBA where α_3 is negative over the complete nematic rage and where the two torques act constructively to develop the instability (the homogeneous distortion cannot exist in materials where the small torque α_3 is positive [16]).

For a H distortion two modes are possible (*see* II). A first mode corresponds to a distortion which is an even function of z and a second one to a distortion odd function of z. An essential point in the discussion of II is the prediction of the existence of a transverse velocity component $v_x(z)$ due to the anisotropy of the viscous tensor. In the case of the first mode which has also been discussed independently by Leslie [4], the transverse velocity is an odd function of z: a wide roll is formed across the sample thickness and transversely to the main flow. In paragraph 2.3 we indicate the observation of a transverse flow changing its sign as one goes across the cell in agreement with the case of the first mode. In the case of the second mode (n_y and n_z odd functions of z) a net flow is expected along the x direction $\left(\int_{-d/2}^{d/2} v_x(z)\, dz \neq 0\right)$ flow lines would have to close in the xy plane. This is not observed here although such a situation with a net transverse flow is obtained in the case of a Poiseuille flow [5].

3.2. Roll instability

Unlike the H mode where analytical solutions are obtained, the exact description of the R instability rests on a complicated mathematical procedure which has been developed in [3]. Here we shall concentrate our attention on a simplified presentation which gives the limit behavior in the presence of a magnetic field H_x parallel to the x direction. In this limit the stabilizing role of the elasticity is small compared to that of the field. The approximation comes from a simplification on the dependence of the fluctuations of the director.

Let us consider (*see* II and the appendix) fluctuations of the form:

$$
\begin{aligned}
n_{y,z}(x, z, t) &= n_{y,z}(t)\cos(q_x x)\cos(q_z z),\\
v_{y,z}(x, z, t) &= v_{y,z}(t)\sin(q_x x)\cos(q_z z),\\
v_x(x, z, t) &= v_x(t)\cos(q_x x)\sin(q_z z),\\
p(x, z, t) &= p(t)\sin(q_x x)\sin(q_z z).
\end{aligned}
$$

The instability threshold is given by a balance of the elastic (characterized by the Frank coefficients $K_{1,2,3}$), magnetic (magnetic susceptibility anisotropy χ_a), electric and viscous torques:

$$(1)\quad \Gamma_y = 0 = \left(K_1 q_z^2 + K_3 q_x^2 + \chi_a H^2 - \frac{\varepsilon_a}{4\pi} E^2\right) n_z + \alpha_2 q_x v_z + \alpha_3 (q_z v_x + s n_y),$$

$$(2)\quad -\Gamma_z = 0 = (K_2 q_z^2 + K_3 q_x^2 + \chi_a H^2) n_y + \alpha_2 (q_x v_y + s n_z).$$

We have omitted dynamic terms such as $\gamma_1 \partial n_z/\partial t$, since we suppose, as experimentally observed, that the instability is stationnary. Close to the threshold, the fluctuation is of the type $w(t) = \alpha \exp \lambda t$ with λ real. The value $\lambda = 0$ corresponds to the threshold.

Using force and continuity equations one can eliminate the velocity components in equations (1), (2). System (1), (2) reduces to the two fundamental coupled equations between n_y and n_z, expressing the effective torques acting on variables n_y and n_z:

$$(3)\quad f_y n_y + A s n_z = 0,$$

$$(4)\quad f_z n_z + B s n_y = 0,$$

where

$$(5)\quad f_y = K_2 q_z^2 + K_3 q_x^2 + \chi_a H^2,$$

$$(6)\quad f_z = K_1 q_z^2 + K_3 q_x^2 + \chi_a H^2 - \frac{\varepsilon_a}{4\pi} E^2,$$

$$A = \alpha_2 \eta_3 \frac{q_x^2 + q_z^2}{\beta}, \qquad B = \alpha_3 + (\alpha_2 q_x^2 - \alpha_3 q_z^2) \frac{e_1 q_z^2 - e_3 q_x^2}{f},$$

with

$$\beta = \eta_2 q_x^2 + \eta_3 q_z^2, \qquad f = \eta_1 q_z^4 + (b + b') q_z^2 q_x^2 + \eta_2 q_x^4.$$

Notations are those of II plus the following:

$$\eta_1 - \eta_3 = e_1, \qquad \eta_2 - \eta_3 = e_2, \qquad \eta_3 - d = e_3, \qquad d = b',$$

The above expression (5) for f_y is given in the limit of low shears where the convective term $\rho s v_z$ in the force equation can be omitted. The compatibility condition between (3) and (4) gives the threshold

$$(7)\quad f_y f_z = AB s^2.$$

In the limit $q_x \to 0$ which is the case of the homogeneous instability, and assuming $q_z = \pi/d$ (in order to have a sinusoidal variation of the

fluctuations vanishing on the limiting plates where strong anchoring of **n** is assumed), we obtain the following threshold:

$$sd^2\left(\frac{\alpha_2\alpha_3}{K_1K_2}\frac{\eta_3}{\eta_1}\right)^{1/2}=\pi^2.$$

NOTE. — The form of the left hand side is that of the Ericksen number characterizing the hydrodynamic instabilities in nematics. It is deduced from the form of a Reynolds number for ordinary fluids by replacing the diffusivity of the vorticity by that for the relaxation of the distortion of the form $K\,q^2/\gamma$ where K is an elastic constant and γ a viscous coefficient.

In the case of a R instability the equation (7) which is of fifth order in q_z defines ten roots ($\pm q_z^j$; $j = 1$ to 5), in terms of s and q_x, which characterize the z dependence of the fluctuations

$$w(x, z, t)=\sum_{j=+1}^{+5} A_j \exp i(q_x x+q_z^j z).$$

Generally, for arbitrary values of s and q_x, this solution will not fulfill the boundary conditions $v_x = v_y = v_z = n_x = n_z = 0$ at $z = \pm d/2$. The threshold corresponds to the minimum value $s_c(q_x)$ such that the boundary conditions are fulfilled. The exact two dimensional calculation (II) shows that, at threshold, among the roots of (7), one wave-vector q_z is close to π/d and the others only contribute in thin layers close to the boundaries. A good approximation, as shown in II, is obtained by retaining a single mode with $q_z \simeq \pi/d$. This corresponds to a mode satisfying roughly the boundary conditions on v_y, v_z, n_y, n_z varying as $\cos(q_z z)$ but not on v_x which behaves like $\sin(q_z z)$. The wave vectors different from π/d contribute in the boundary layer in order to make v_x vanish. In this one mode approximation, the threshold corresponds to the minimum shear rate s_c solution of (7). This defines the critical wavevector of the rolls, q_x^c.

As the magnetic field is increased, the wavevector of the rolls, q_x, increases. This result is not obvious since raising H corresponds to increasing the stabilizing torques: the magnetic one varies as H^2 and the elastic one as q_x^2. But one must consider a more precise balance with the viscous torques, including all new effects such as "focusing" forces due to the roll distortion, in order to get this dependence. A complete analysis of the q_x dependence on H has been developed in [3].

Large magnetic field behavior

For a large magnetic field such that $q_x^2 \gg q_z^2$ one can expand expression (7) in powers of $(q_z/q_x)^2$. Assuming an isotropic elasticity ($K_1 = K_2 = K_3 = K$), and no electric field, a first order expansion gives:

$$s^2 = \frac{\{K(q_x^2+q_z^2)+\chi_a H^2\}^2}{(\alpha^*)^2}\left(1+2\lambda\left(\frac{q_z}{q_x}\right)^2\right) \tag{8}$$

with

$$\alpha^{*2} = \alpha_2'\alpha_3' \qquad \text{and} \qquad 2\lambda = \mu - \frac{e}{\eta_2};$$

$$\alpha_2' = \frac{\alpha_2\eta_3}{\eta_2}; \qquad \alpha_3' = \alpha_3 - \alpha_2\frac{e_3}{\eta_2};$$

$$-\alpha_3'\mu = \frac{\alpha_2 e_3}{\eta_2}\left\{\frac{\alpha_2 e_1+\alpha_3 e_3}{\alpha_2 e_3}+\frac{b+b'}{\eta_2}\right\}.$$

For MBBA at 25°C [15] we obtain $\alpha^* = 0.21$ P; $2\lambda = 1.47$.

Let us measure the length in units of the thickness d and define dimensionless wave vectors $\tilde{q}_x = dq_x$; $\tilde{q}_z = dq_z$. The shearing rate is characterized by an Ericksen number:

$$\mathrm{Er} = \frac{sd^2\alpha^*}{K}, \tag{9}$$

and the intensity of the magnetic field by:

$$F = \frac{\chi_a H^2 d^2}{K}, \tag{10}$$

F is a measure of the ratio of the applied field to the characteristic field one would need to distort the structure in a Freedericks experiment.

Equation (8) may be written in a dimensionless fashion

$$\mathrm{Er} = [\tilde{q}_x^2+\tilde{q}_z^2+F]\left[1+\lambda\left(\frac{\tilde{q}_z}{\tilde{q}_x}\right)^2\right].$$

The threshold is obtained for $\tilde{q}_x^c$ such that $d(\mathrm{Er})/d(\tilde{q}_x^2) = 0$.

This leads to:

$$(\tilde{q}_x^c)^4 = \lambda\tilde{q}_z^2(\tilde{q}_z^2+F). \tag{11}$$

For large field H, one obtains:

$$(\tilde{q}_x^c)^4 \propto F = \frac{\chi_a H^2 d^2}{K}$$

and a dependence

$$\tilde{q}_x^c \propto \sqrt{H d} \text{ or } \left(\frac{d}{\lambda}\right)^{1/2} \propto H d \tag{12}$$

and

$$Er_c \sim \frac{\chi_a H^2 d^2}{K} \tag{13}$$

3.3. Experiments

(a) *Thresholds*

The measurements of thresholds are done in the cylindrical arrangment. They are given in terms of the critical angular velocity of the inner cylinder on Figure 4. A stabilizing magnetic field parallel to the axis of the cylinder (the unperturbed molecular direction is obtained by surface treatment) is applied. The existence of two different solutions as the magnetic field is varied is clearly seen from the inset of the Figure. The low field data, where an homogeneous instability (H. I.) is met at threshold, were obtained by keeping the shear rotation constant and decreasing the field. When the field becomes smaller than a critical value the capacitance of the quadrupolar arrangment begins to increase linearly thus providing an accurate estimate of threshold. The linear variation is consistent with a variation of the twist–axial–distortion with shear $n_\varphi = N\,(s-s_c)^{1/2}$: the capacitive experiment detects changes of the effective dielectric constant proportional to n_φ^2 near the distortion threshold. The justification for the 1/2 exponent corresponding to a "mean field" like behavior has recently been given by P. Manneville [17] who has also obtained the explicit form of N from a non linear analysis of the homogeneous mode.

In large magnetic fields, a roll instability (R. I.) mode is obtained at threshold

The two instabilities are well described on Figure 4 by two branches linear in H^2. This form of dependence is expected for the H mode (I) as well as for the R mode as was discussed above [formula (13)]. The exact two dimensional analysis of reference II can also be fitted to these results. We can rescale the exact calculation of Figure 6 of II, which

corresponds to our Figure 4, by using reduced units $H\,d$ for the field and sd^2 (i. e. a term proportional to the Ericksen number) for the shear. (The coefficients used in the numerical calculations were also obtained from Gähwiller [15] work.) There is an excellent quantitative agreement with theory. The straight line (Th.) represents the result of the asymptotic calculation and there is not much deviation from a straight variation down to low field (the $\times$ represents an exact calculated point). The calculated value of the crossover field is given by $H\,d \sim 18.8$ whereas the experimental

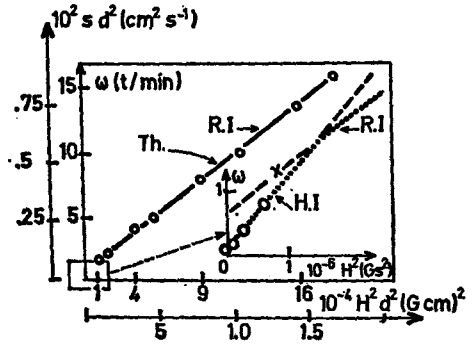

Fig. 4. — This figure gives the experimental results on a cylindrical cell ($D_i = 3.4$ mm; $D_0 = 4$ mm) of threshold. The stabilizing field is along the cylinder axis. These results are compared with theory (asymptotic straight line form and point $\times$) in normalized coordinates sd^2, $H^2\,d^2$.

one is $H\,d \sim 30$. The agreement is good if one realizes that it is given rather inaccurately both theoretically and experimentally by the intercept of two straight lines of close slopes. A word of caution should be given concerning the meaning of a quantitative fit: the elastic constants are known in materials like MBBA with a large dispersion (20 %). This is due largely to the poor stability of this compound between or even during our experiments. This is also true for the viscous terms (our determinations are very consistent with those given in reference [15]. Notice from (7) that a small change of the α_3 viscosity term modifies strongly the homogeneous threshold but not the roll one.

(b) Wavelength

The wavelength dependence in the R. I. regime as a function of H has been measured using a microscope observation. Figure 5 gives this

variation in reduced units $(d/\lambda)^2$ versus $(H\,d)$. For low fields, λ is of the order of the thickness. It decreases as $H^{-1/2}$ in large fields. This asymptotic behavior agrees qualitatively and quantitatively with the theoretical description given above [formula (11), (12)]. The fit is also given for low fields where we have used the numerical results of II.

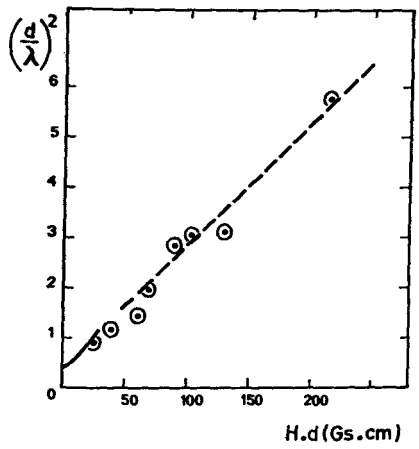

Fig. 5. — The circles are experimental measurements of wavelength of the R. I. mode in continuous shear, right at threshold. The straight line gives the asymptotic theoretical behavior whereas the solid curve gives the result of the numerical calculation. Note however that the R. I. does not extend down to $H\,d = 0$.

The good agreement on thresholds and wavelength over the whole range of fields between the experiments and the theory based on the Leslie-Ericksen hydrodynamic description may be considered as an indication of the validity of this theory. However, in order to verify more completely the form of the Leslie-Ericksen tensor, one should check the exactness of the sd^2 parametrization by varying the thickness d over a large enough range [18] (2).

(2) One of us (E.G.) wishes to thank F. M. Leslie for pointing out to him the various implications concerning the validity of the shape of stress tensor as coming from various flow experiments.

4. Alternating flow

4.1. Linear model

Experiments with alternating shear show that, except for very low frequencies, the roll instability is preferred to the H one even in the absence of a stabilizing magnetic field. This can be understood by the simple following argument: in the torque equations, the viscous torque terms $\gamma\, \partial n_{y,z}/\partial t$ play a role similar to the term $\chi_a\, H^2\, n_{y,z}$ and are also independent of the wave vectors q_x, q_z. The time constant for the relaxation of the distortion under a field H is $T_0\,(H) = \gamma/(\chi_a\, H^2)$. γ is a rotational viscosity and damps the effect of the magnetic torque A magnetic field of 10^3 G, corresponding to the cross over between the H and R regime, will correspond to a cross over frequency $\nu \sim T_0^{-1}\,(H) \sim 3$ Hz. This value corresponds well to the limit between H and R instabilities. In the following we shall only consider the R regime.

Since the velocities relax much more rapidly than the orientation variables, the motion of the director is obtained by including the director relaxation in the torque equations (3), (4) (the forces equations are unchanged since we can neglect terms such as $\rho\, \dot{v}$):

$$\gamma_y \dot{n}_y + f_y n_y + A\, s n_z = 0,$$
$$\gamma_z \dot{n}_z + f_z n_z + B\, s n_y = 0,$$

with

$$\begin{cases} \gamma_y = \gamma_1 - \alpha_2^2\, q_x^2/\beta \\ \gamma_z = \gamma_1 - (\alpha_2\, q_x^2 - \alpha_3\, q_z^2)^2/f \end{cases}$$

or

$$\dot{n}_y + \frac{n_y}{T_y} + A'\, s n_z = 0, \tag{14}$$

$$\dot{n}_z + \frac{n_z}{T_z} + B'\, s n_y = 0, \tag{15}$$

with

$$T_y = \frac{\gamma_y}{f_y}, \qquad T_z = \frac{\gamma_z}{f_z}, \tag{16}$$

$$A' = \frac{A}{\gamma_y}, \qquad B' = \frac{B}{\gamma_z}. \tag{17}$$

Here s depends explicitely on the time variable t.

The $\gamma_{y,z}$ are effective rotational viscosities and $T_{y,z}$ are time constants for the spontaneous relaxation of the distortion characterized by $n_{y,z}$ components.

The time variation of the variables $n_y(t)$ and $n_z(t)$ coupled with a variable shear term $s(t)$ can be simulated analogically. This was done in an independent work [19] and was found to give a variation of threshold in excellent agreement with the analytical solution obtained with a square wave excitation (I). The analogical solution has also the merit of displaying the characteristic functions [feedback coupling (A, B) and damping $(1/T_{y,z})$] in an analogical electronic description applicable to many instabilities.

We shall consider mainly two types of periodic excitations ($T = 2\pi/\omega$):

(i) sine waves (denoted as $\sim$) of the form $s(t) = \bar{s}\sqrt{2}\cos\omega t$;

(ii) square wave signal (denoted as $\square$) corresponding to a saw-tooth displacement of the upper plate

$$s(t) = +\bar{s}, \qquad 0 < t < \frac{T}{2},$$

$$s(t) = -\bar{s}, \qquad \frac{T}{2} < t < T.$$

Considering equations (14) and (15), one sees that the solutions are of one of the two following types:

Y mode where $n_y\left(t+\frac{T}{2}\right) = -n_y(t)$; $\quad n_z\left(t+\frac{T}{2}\right) = n_z(t)$;

Z mode where $n_z\left(t+\frac{T}{2}\right) = -n_z(t)$; $\quad n_y\left(t+\frac{T}{2}\right) = n_y(t)$.

The effect of fields has been discussed at length in reference [1]. The decrease of the relaxation time constant T_z due to a stabilizing high frequency electric field E_z as well as the decrease of T_y and T_z due to a stabilizing field H_x can be included in the variation of the dimensionless ratios T_y/T_z and ωT_y, which characterize the time constant effects. They lead to change in the threshold value and also to an interchange of mode from Y (only n_y goes through zero over one period of the flow) to Z (same for n_z). Here we will complement this study under three aspects:

(i) we will give a better description of the thresholds;

(ii) we will compare the response to different alternatingsi gnals;

(iii) we will extend the diagram using the effect of a low frequency field.

4.2. QUALITATIVE DESCRIPTION

Let us first ignore the time dependence of the parameters T_y and T_z and consider T_y and T_z as constants. This is only true for low shears where the convective term in the force equation can be omitted. A simple analysis allows us to interpret qualitatively the shape of the experimental instability curve of Figure 8. Consider, for simplicity, a square shape signal. We take n_y and n_z positive at the initial time $t = 0$ where we

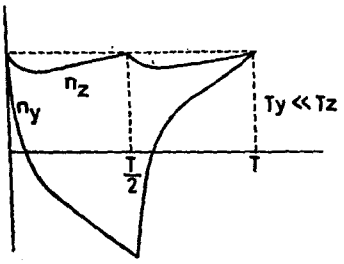

Fig. 6. — Fluctuations of n_y and n_z at the threshold E_{10} of Figure 18 in the Y regime. When the shear is reversed at $t = 0$, n_y decays more rapidly than n_z for $T_y \ll T_z$. When n_y changes sign, the source term causes n_z to increase.

reverse the sign of the shear. This induces a change of sign of the source terms in equations (14), (15) and n_y and n_z begin to decrease (the variation of n_y and n_z with time is given on Fig. 6). For $T_y \ll T_z$, n_y relaxes much much more rapidly than n_z and goes through zero first. Then the source term in (15) turns out to be positive and n_z starts increasing, its amplitude growing up to $t = T/2$ where the signal is again reversed. At the start of each period there is a lossy time ($\sim T_y$) where the source term does not contribute to the amplification of the n_z fluctuation. Increasing T_y broadens this region and there is less and less amplification of n_z. In this Y regime we can assume that n_y oscillates whereas n_z is nearly constant except when T_y approaches T_z.

For $T_y = T_z$ one sees easily that both fluctuations decay to zero at the same rate: the system is always stable.

For $T_z \gg T_y$ we have a Z regime similar to the Y one but where n_z plays the role of n_y in the previous case and oscillates through zero.

4.3. THRESHOLDS

We consider first the Y regime. Integration of (15) leads to

$$n_z(t) = -B' \exp\left(\frac{-t}{T_z}\right)\int_{-\infty}^{t} n_y s(t') \exp\frac{t'}{T_z}\, dt'. \tag{18}$$

For $T_z \geqslant T$, $\exp(t'/T_z)$ may be considered as constant over one period. This corresponds to a first harmonic approximation.

For a *sinusoidal* excitation it leads to

$$n_z(t) = \bar{n}_z = -B' \frac{T_z}{T} \bar{s} \sqrt{2} \int_0^T \cos\omega t . n_y(t)\, dt, \tag{19}$$

one deduces n_y from (14):

$$n_y(t) = -\exp\left(\frac{-t}{T_y}\right) A' \bar{s} \sqrt{2}\, \bar{n}_z \int_{-\infty}^{t} \cos\omega t' . \exp\left(\frac{t'}{T_y}\right) dt'. \tag{20}$$

By integration it gives:

$$n_y(t) = -A' \bar{s} \sqrt{2}\, \bar{n}_z T_y \frac{(\cos\omega t + T_y \omega \sin\omega t)}{1+\omega^2 T_y^2},$$

The compatibility with equation (19) leads to the threshold expression:

$$\frac{\bar{s}^2 A' B' T_y T_z}{1+\omega^2 T_y^2} = 1, \tag{21}$$

for the Y mode. Let us emphasize that this expression implies not only the condition $T_z \gg T$ but also the condition $T_z > T_y$ since the system chooses the solution where only n_y oscillates.

For a *square wave* signal one obtains for the Y regime:

$$\bar{n}_z(t) = \bar{n}_z = -2B' \frac{T_z}{T} \bar{s} \int_0^{T/2} n_y(t')\, dt', \tag{22}$$

$$n_y(t) = C \exp\left(\frac{-t}{T_y}\right) - A' \bar{s} T_y \bar{n}_z, \tag{23}$$

where

$$C = \frac{2A' \bar{s} T_y \bar{n}_z}{(1+\exp(-T/2T_y))},$$

is determined by writing the condition $n_y(t+T/2) = -n_y(t)$ for $t = 0$.

The compatibility between (22) and (23) gives the threshold:

$$A' B' \tilde{s}^2 T_y T_z \left(1 - \frac{\tanh(T/4T_y)}{T/4T_y}\right) = 1. \tag{24}$$

The thresholds of the Z mode are obtained by changing T_y and T_z leading to expressions valid when $T_y \gg T$ and $T_y > T_z$.

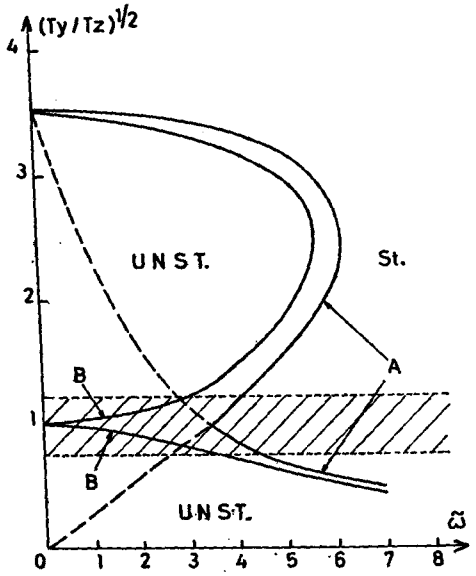

Fig. 7. — Threshold curves drawn, for a constant shear, as a function of the reduced frequency $\tilde{\omega} = \omega T_y$. The part to the left of the curve is unstable. Curve A corresponds to the theoretical simplified model. Curve B corresponds to analogical and numerical solutions of equations (7) and (8).

Figure 7 gives different determinations of the instability threshold in units $(T_y/T_z)^{1/2}$ and reduced frequency $\tilde{\omega} = \omega T_y$. At first sight the Z and Y mode do not seem to contribute in a symmetric way. This is only due to the nature of the plot. The two regimes will appear similar if one will plot the shear s as a function of the frequency. Curves A correspond to the "first harmonic" description given above for a sine wave excitation and for the Y mode (19). The curve B is the analogical solution of (14) and (15) and is indistinguishable from that of a numerical integration of the same equations, which we have also performed. The cusp extending

to zero on this curve and associated with the impossibility of instability when $T_y/T_z = 1$, is not reproduced on the curve A. Indeed we have assumed in the first harmonic model that $T_z > T_y$ ($T_y > T_z$) in the Y (Z) regime then one cannot expect the two curves to be similar in the intermediate regime ($T_y \sim T_z$).

A comparison can also be made between different types of excitations.

Let us define the effective shear by

$$\bar{s}^2_{\sim} = \frac{\pi^2 D^2_{\sim} f^2}{2d^2}, \quad \text{for a sine wave,} \tag{25}$$

$$\bar{s}^2_{\square} = \frac{4 D^2_{\square} f^2}{d^2}, \quad \text{for a square wave} \tag{26}$$

where D is the total displacement.

The numerical and analogical solutions indicate that the curves are practically the same for both types of excitations provided $\bar{s}^2_{\sim} = \bar{s}^2_{\square}$.

The behavior is also apparent on equations (21) and (22) giving the thresholds for the two types of excitations. We consider the two limits:

(i) $\omega \to 0$:

The two expressions lead to the same result:

$$A' B' \bar{s}^2 T_y T_z = 1 \quad \text{or} \quad f_y f_z = AB s^2;$$

(ii) $\omega \to \infty$:

$$\frac{\bar{s}^2_{\sim} A' B' T_z}{\omega^2 T_y} = \frac{\bar{s}^2_{\sim} A' B' T_z T^2}{4\pi^2 T_y} = 1; \tag{27}$$

$$\frac{\bar{s}^2_{\square} A' B' T_z T^2}{48 T_y} = 1. \tag{28}$$

The two results differ by less than five per cent.

In fact we have checked, using our analogical solution, that this result applies also quite generally for different shapes of signals (square, triangular...) indicating that only the average shear is important at least as long as the period of the signal is short enough compared with the time constant of orientation. In the opposite limit, the distortion would come to equilibrium with the instantaneous value of the shear and the alternating problem loses interest. The cusp shape variation agrees with the theoretical analysis of section 3. We may also note the difference

with the electrohydrodynamic instability (E. H. D.) case [20]. In this problem it was found both experimentally and theoretically that the instability curves (electric field versus frequency) corresponding to our variation of Figure 18 were quite different for both types of excitation. However in this problem the time constant itself is a function of the instantaneous value of the destabilizing force (the alternating electric field) and the relaxation process should adjust to it during the course of a period. In the present problem the relaxation time constants of the director are independent of the shear rate (and averaging is completely consistent) at least as long as the convective contribution can be neglected. In fact, as it is shown in the appendix, this term is negligible for the frequencies of the excitation used in this study. If not, one would expect a behavior very similar to the electrohydrodynamic instabilities where one relaxation time depends on the applied excitation.

4.4. Experiments and discussion

(a) *Threshold*

The variation of intensity of one of the intense diffraction peaks is used to obtain an accurate determination of the R threshold. We consider here only this determination and will study in an independent work [13] some properties above threshold that are obtained from the diffraction experiment. One can adjust the values of the coefficients T_y and T_z [*see* (16), (5), (6)] by the application of an electric and magnetic field.

In a given experiment, the magnetic field as well as the shear are kept constant. For a given frequency (f_0 on *Fig.* 8), where, in zero electric field, a Y instability mode is obtained, a diffracted intensity is recorded. As the high frequency electric field (or voltage V) is increased from zero, the intensity decreases continuously to zero for a value E_{I0}. A new diffracted intensity is measured above a field E_{0II}. For a much large value E_{II0}, it decreases again to zero.

The cusp in the instability diagram is related to the change of regime between the two parts of the diagram shown on Figure 8.

We have used experimentally both a sinusoidal and square wave shear. A given curve is characterized by a constant value of the effective shear $\bar{s}$ defined by (25), (26). The points given on the curves for the two modes of excitation are such that: $\bar{s}^2_{\sim} = \bar{s}^2_{\square}$ for the two experiments.

The two variations are nearly identical. — The comparison was extended as a function of a stabilizing magnetic field H from 1 to 2.5 kg and no systematic deviation from this simple remarkable result has been obtained.

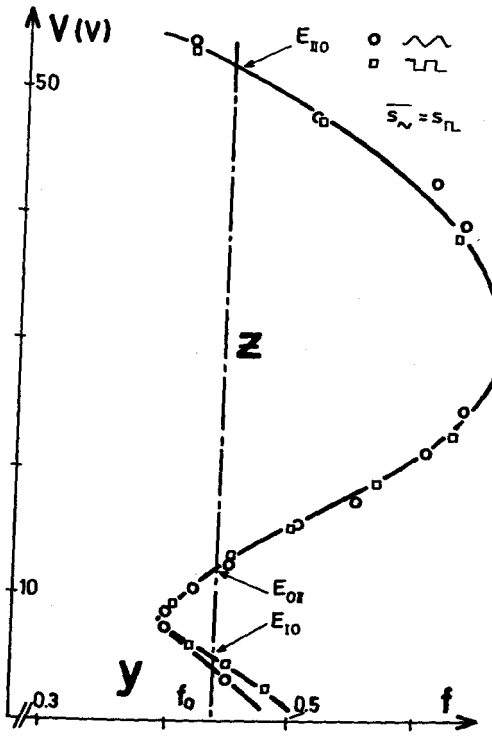

Fig. 8. — Experimental threshold curve for both sinewave and square wave excitation. The part to the left is the domain of existence of the Y and Z roll instabilities.

This behavior agrees with the analysis given in the previous paragraph.

Experimentally one observes on Figure 8 curves similar to A curves of Figure 7 and not to B ones but this is fortuitous. In fact, the previous solution (A) did not take into account the explicit dependence on the wavevectors q_x and q_z. If one introduces this variation in the sames implified way as for the continuous shear with $q_z = \pi/d$ fixed and q_x free to vary, one obtains curves very similar to the experimental ones. Figure 9 gives a set of calculated curves in E units as a function of the reduced

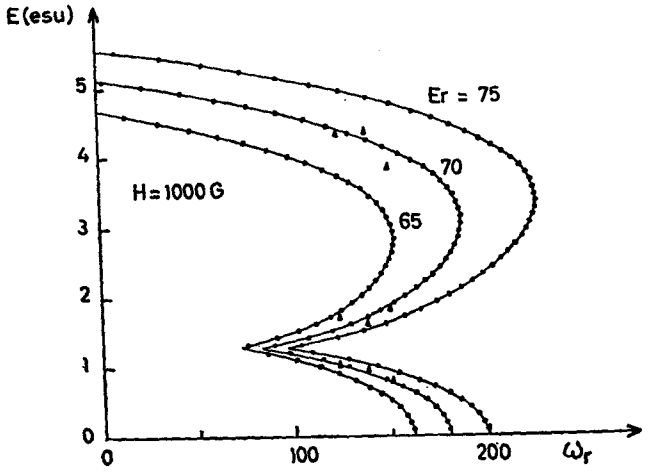

Fig. 9. — Critical electric field E in esu as a function of the reduced frequency $\omega_r = (\gamma_1 d^2/4 K_1) 2 H f$.

The experimental points (Δ) correspond to an Ericksen number

$$Er = (sd^2/4)(\alpha_2 \alpha_3/K_1 K_2)^{1/2} = 75$$

(calculated from Gähviller data on MBBA at 25°C). We see that small (less than 5 %) adjustment on Er and on the ratio K/γ_1 would give on excellent quantitative fit with the theory.

frequency $\omega_r = (\gamma_1 d^2/4 K_1) \omega$ for various of the Ericksen number defined by:

$$Er = \frac{sd^2}{4}\left\{\frac{\alpha_2 \alpha_3}{K_1 K_2}\right\}^{1/2}.$$

Some experimental points are also given which correspond to an Ericksen number equal to 75 (calculated using data of reference [15]). The points fall on the calculated curve Er = 70. The 5 % discrepancy is not significant and well within the errors on the viscoelastic coefficients.

For low Er numbers we also obtain that the cusp disappears progressively, in agreement with the experiments (see *Fig.* 7 of I; *see* also *Fig.* 14 of this article). However the field of the cusp is rather insensitive to the value of Er.

(*b*) *Wavelength*

The Figure 10 reproduces the curve Er = 70 of Figure 9 and indicates the calculated wavelength of the rolls along the threshold curve. Experimentally one also observes, in qualitative agreement with this

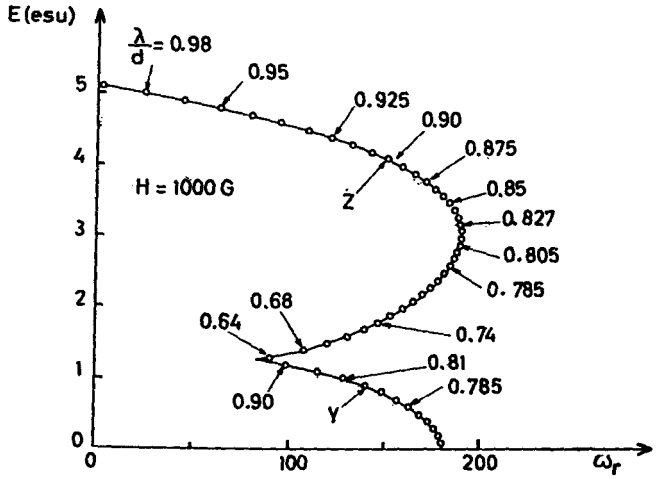

Fig. 10. — Numerical calculation of the variation of the reduced wavelength along the instability curve calculated for Er = 70. It is found that the cusp disappears for small Er, in agreement with experimental results of (1).

result, that in the Y regime the wavelength is nearly constant whereas it increases markedly with field in the Z regime. Let us consider the ratio of the wavelengths at points I0, 0II et II0 for the same frequency (see *Fig.* 8). One observes a good agreement between experimental values (exp) and the theoretical ones (th).

$$\left(\frac{\lambda_{0II}}{\lambda_{I0}}\right)^{exp} = 1, \qquad \left(\frac{\lambda_{0II}}{\lambda_{I0}}\right)^{th} = 1.07,$$

and

$$\left(\frac{\lambda_{II0}}{\lambda_{I0}}\right)^{exp} = 0.85, \qquad \left(\frac{\lambda_{II0}}{\lambda_{I0}}\right)^{th} = 0.88.$$

NOTE. — The variation of diffracted beam intensity around E_{0II} and E_{II0} on Figure 8 are very steep. This variation is very similar to that obtained in the Poiseuille geometry, as given in Figure 12 of [5]. In both cases this relatively sharp variation at E_{0II} and E_{II0} is also associated with a small hysteresis in the determination of critical values. This result is not understood at present. It would be of interest to know if this is a property of the Z regime by itself or if it is due to the presence of an electric field by having a nematic where the Z regime is obtained in zero electric field. The hysteresis suggests a mechanism with an inverse

bifurcation (*see* for example [21]) ([3]). It is known in this case that the threshold measured when starting progressively and carefully from an undistorted state corresponds to the solution of the linear problem. This procedure was used to obtain the results of Figure 8. In practice, the hysteresis is rather small in the experiments and the agreement with the predictions of a linear model suggests that the non linearities associated with this sharp transition are not too severe.

4.5. HIGH FREQUENCY SHEAR

Let us suppose that the elasticity is isotropic and that no electrical field is applied. Then we get using (5), (6) and (16):

$$f_y = f_z; \qquad \frac{T_y}{T_z} = \frac{\gamma_y}{\gamma_z}.$$

We will consider the high frequency limit with $(q_z/q_x)^2 \ll 1$. With this approximation we get:

$$\gamma_y = \gamma^*\left(1+\lambda_y\left(\frac{\tilde{q}_z}{q_x}\right)^2\right), \qquad \gamma_z = \gamma^*\left(1+\lambda_z\left(\frac{\tilde{q}_z}{\tilde{q}_x}\right)^2\right),$$

with:

$$\gamma^* = \gamma_1 - \frac{\alpha_2^2}{\eta_2}, \qquad \lambda_y = \frac{\alpha_2^2\eta_3}{\eta_2^2\gamma^*}, \qquad \lambda_z = \frac{\alpha_2^2}{\eta_2\gamma^*}\left(\frac{2\alpha_3}{\alpha_2} + \frac{b+b\eta}{\eta_2}\right).$$

Consequently

$$\frac{T_y}{T_z} \simeq 1+(\lambda_y-\lambda_z)\left(\frac{\tilde{q}_z}{\tilde{q}_x}\right)^2.$$

Typical values for MBBA at 25°C are: $\gamma^* = 0.18$ P, $\lambda_y = 1.35$, $\lambda_z = 4.44$. As $\lambda_y < \lambda_z$, this implies $T_y < T_z$ and one expects, for $E = 0$, a Y regime as observed experimentally.

([3]) Up to now there has been no attempt to describe the non linear hydrodynamic problem in the case of the roll instability. Such a discussion should include convective contributions which are here negligible.

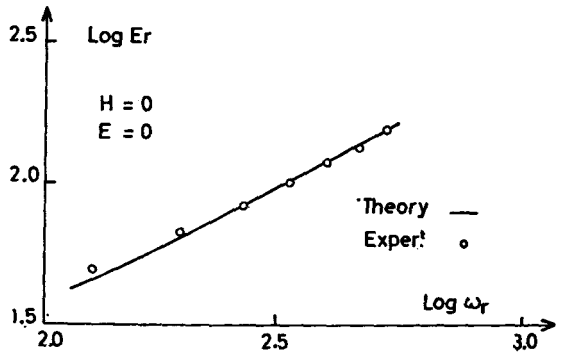

Fig. 11. — Plot of the Ericksen number Er : $(sd^2/4)(\alpha_2\,\alpha_3/K_1\,K_2)^{1/2}$ as a function of the reduced frequency ω_r.

The theoretical curve is the exact calculation for a square excitation. A slight adjustement of the vertical scale has been done when starting from Gähviller data. Experimental points apply to exactly the same situation as the theory.

If one expands equation (21) in terms of powers of $(q_z/q_x)^2$ one gets:

$$\bar{s}^2(\omega) = \frac{f_y^2}{AB} + \frac{\omega^2\gamma_y^2}{AB} = \bar{s}^2(0) + \omega^2\frac{\gamma^{*2}}{\alpha^{*2}}\left(1+2(\lambda_y+\lambda)\left(\frac{\tilde{q}_z}{\tilde{q}_x}\right)^2\right) \tag{29}$$

or:

$$\mathrm{Er}^2(\omega) = \mathrm{Er}^2(0) + \omega^2\tau^2\left(1+\lambda'\left(\frac{\tilde{q}_z}{\tilde{q}_x}\right)^2\right),$$

where $\tau = \gamma^* d^2/K$ is the relaxation time of an orientation fluctuation of wavelength d; $\lambda' = 2(\lambda_y+\lambda)$.

A typical value in MBBA at 25°C is $\tau \simeq 70$ s for $d = 200\,\mu$.

The threshold condition $d\mathrm{Er}/dq_x(\omega) = 0$ leads to the relation:

$$(\tilde{q}_x^2+\mathrm{F})(2\tilde{q}_x^4+\lambda\tilde{q}_z^2\tilde{q}_x^2-\lambda\tilde{q}_z^2\mathrm{F}) = \omega^2\tau^2\lambda'\tilde{q}_z^2. \tag{30}$$

In the one mode approximation using $q_z = \pi/d$, relation (30) leads to the variation of the wave vector component q_x as a function of ω. The highest order contribution gives:

$$2\tilde{q}_x^6 \propto \omega^2\tau^2\lambda'\tilde{q}_z^2 \quad \text{or} \quad \tilde{q}_x \propto (\omega\tau)^{1/3}, \tag{31}$$

and

$$\mathrm{Er}^2 \propto \omega^2\tau^2. \tag{32}$$

Figure 11 gives a comparison between the experimental and calculated variation. We note in particular the wide range of validity of the approximate form (32).

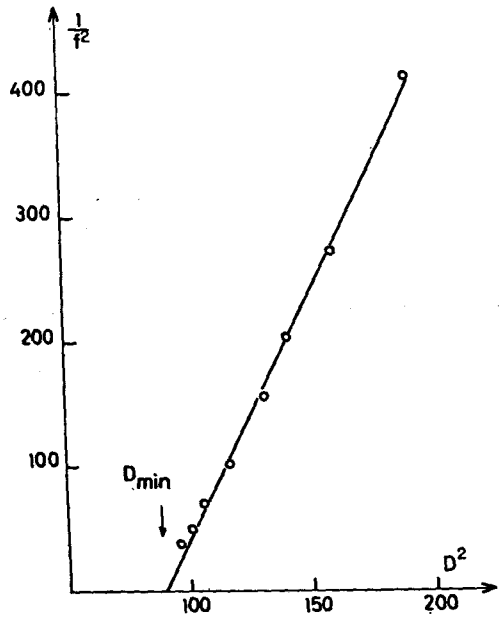

Fig. 12. — The extrapolation of the minimum displacement required to produce an instability at infinite frequency gives a determination in agreement with that deduced from equation (33).

We can write the asymptotic expansion for the critical shear rate using the amplitude of the displacement D, which is a physical variable adjusted in the experiments. For a sine wave excitation D is given by

$$\frac{D\omega}{d} = 2\sqrt{2\bar{s}}.$$

In the limit of very high frequency the critical shear rate can be expressed in term of the existence of a minimum displacement (independent of ω) needed to produce the instability: D_{min} is given from (29) by

$$\frac{D_{min}}{d} = 2\sqrt{2}\frac{\gamma^*}{\alpha^*}. \tag{33}$$

In Figure 12 we give a direct measurement of the amplitude of displacement as a function of the frequency of the shear in units D^2, f^{-2}. The linear variation agrees with formula (29). The minimum displacement $D_{min} = 1.1$ mm is in reasonable agreement with a theoretical determination $D_{min} = 0.7$ mm.

The result is insensitive to the value of the magnetic field (2,100 G in the first experiment; 3,200 G in the second one). Experimentally an increase of field from 1.5 kG to 3.3 kG leads to an increase of the minimum displacement by 10 %.

The fact that the displacement rather than the shear characterizes the threshold for high frequency can be analysed in relation with acoustics. The large displacements involved for the instability described here ($\sim$ mm) are far beyond the reach of usual shear wave experiments such as produced by piezoelectric transducers. One should not expect to be able to produce a R. instability similar to that described here. However, for large frequencies the viscous penetration depth $\delta = (\alpha_4/\rho\omega)^{1/2}$ is smaller than the sample thickness (whereas our experiments were done in the limit of a uniform shear such that $d \ll \delta$): the distortion induced by the flow takes place over a reduced distance. This in turn may reduce the orientation time constant and favor the instability. A more complete study could be carried as an extension of the work of Candau and Martinoty [22]. Scudieri [23] has recently obtained roll instabilities with rolls *perpendicular* to the shear starting from an *homeotropic* sample sheared at a frequency of 7.46 kHz with displacement thresholds of the order of 5×10^{-2} μ. The geometry as well as the planform of the rolls indicate a fairly different problem from the one discussed here. Very recently, we have considered experiments in the same homeotropic geometry using an audiofrequency excitation. Instabilities apparently quite similar to those reported in Scudieri's work and with very low thresholds were obtained. However, the presence of an elliptically polarized (rather than just linearly) shear appear to be indispensible to produce the convective instability.

4.6. Effects of a low frequency electric field

The analogy between the system of rolls produced in a shear and that obtained under the influence of a low frequency electric field E_l (Williams domains) [14] suggests that the two mechanisms could be superimposed in a single experiment.

In a shear flow, an initial fluctuation of n_z, periodic along x, induces a periodic distortion of n_y which, in turn, causes a flow in the z direction, $v_z(x)$. On the other hand, when a low frequency electric field is applied, the fluctuation of n_z creates space charges which, *via* the electrostatic forces, also induce a velocity $v_z(x)$. In both cases, in MBBA,

the velocity v_z reinforces the distortion and is the main contribution to the development of the rolls.

The velocity $v_z(x)$ can in fact be induced partly by the shear, partly by a low frequency electric field. We expect that the critical shear should decrease when a low frequency field is applied.

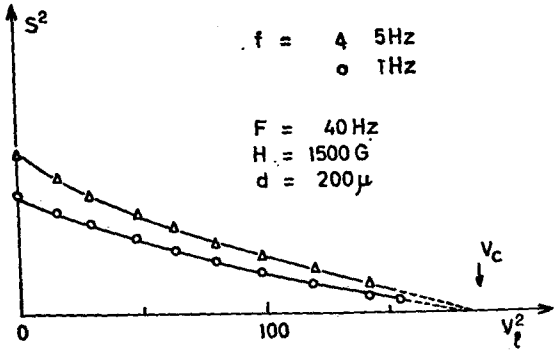

Fig. 13. — This figure gives the decrease of the critical shear rate as a low frequency (F = 40 Hz) voltage $V_l = E_l d$ is increased. The decrease is given for two shear frequencies $f = .5$ Hz (Δ) and 1 Hz (0).

On Figure 13, experimental data are presented at two different shear frequencies. The square of the threshold of the shear decreases roughly linearly as a function of the square of the applied voltage. A small deviation is found from this behavior near V = 0. The shear becomes zero for V_c, i. e. for the critical voltage needed to induce Williams domains.

A simplified quantitative description can be found, based on the one-dimensional analysis of roll-instabilities recalled in the theoretical chapter. We suppose that the frequency F of the electric field is low enough to produce Williams domains but high enough so that, during one period of the field, n_z and n_y can be taken as constants (for e. g. 40 Hz and 200 μm cell thickness, these assumptions are correct). In this case a simple calculation gives a set of equations equivalent to (14) and (15) with:

$$\frac{1}{T_y} = \frac{1}{T_{y0}} + \frac{\chi_a H^2}{\gamma_y}, \tag{34}$$

$$\frac{1}{T_z} = \frac{1}{T_{z0}} + \frac{\chi_a H^2}{\gamma_z} - \frac{\alpha E_l^2}{4\pi\gamma_z}; \tag{35}$$

E_l^2 is the applied low frequency field; α is an effective dielectric constant taking into account the effective conductivities, dielectric constants and

viscosities [14]. It is positive for MBBA: a low frequency field, smaller than the Williams threshold, increases T_z.

When T_z/T_y is sufficiently smaller than 1, the square of the critical shear is proportional to $1/T_z$ [1]. As $1/T_z$ decreases linearly with V_l^2, we expect the square of the shear threshold to decrease also linearly with V_l^2, as observed experimentally on Figure 13.

The effect of a low frequency can be compared with that of a high frequency one E_h. For the latter case we must replace in (14) and (15), the expression (35) by

$$\frac{1}{T_z} = \frac{1}{T_{z0}} + \frac{\chi_a H^2}{\gamma_z} - \frac{\varepsilon_a E_h^2}{4\pi\gamma_z} = \frac{1}{\bar{T}_{z0}} - \frac{\varepsilon_a E^2}{4\pi\gamma_z} \tag{36}$$

and retain the expression (34) for T_y. The ration $|\alpha/\varepsilon_a|$ is of the order of 1 in MBBA (4). It can be determined by applying simultaneously a low and high frequency field and measuring the ratio of the two fields at which their effects compensate (i. e. at which the shear threshold is the same as without field). The ratio $T_y/\bar{T}_{z0}$ can be also determined by the following method:

In the simple one dimensional analysis (I), the cusp is given by $T_z = T_y$, or

$$\frac{1}{\bar{T}_{z0}} - \frac{1}{T_y} = \frac{\varepsilon_a}{\gamma_z} E_{cusp}^2 . \tag{37}$$

At the critical field for Williams domains, E_c, we have $T_z^{-1} = 0$ and

$$\frac{1}{\bar{T}_{z0}} = \frac{\alpha E_c^2}{\gamma_z} . \tag{38}$$

From (37) and (38) we get

$$\frac{T_y}{\bar{T}_{z0}} = \left(1 - \frac{\varepsilon_a E_{cusp}^2}{\alpha E_c^2}\right)^{-1} .$$

(4) The threshold for the Williams domain is given by $\alpha E_l^2 - q_x^2 K_1$ whereas that for a Freedericksz transition on an homeotropic sample is

$$|\varepsilon_a| E_F^2 = \left(\frac{\pi}{d}\right)^2 K_3 .$$

Thus

$$\frac{\alpha}{|\varepsilon_a|} \sim \left(\frac{E_F}{E_l}\right)^2 \frac{K_1}{K_3} \frac{q_x^2 d^2}{\pi^2} .$$

In MBBA, these three ratios are found experimentally to be of the order of unity.

Now it is possible to determine T_y/T_z for an arbitrary field:

$$\frac{T_y}{T_z} = \frac{T_y}{T_{z0}}\left(1 - \frac{V_l^2}{V_c^2}\right) \text{(low frequency)},$$

$$\frac{T_y}{T_z} - 1 = \left(\frac{T_y}{T_{z0}} - 1\right)\left(\frac{V_h^2}{V_{cusp}^2} - 1\right) \text{(high frequency)}.$$

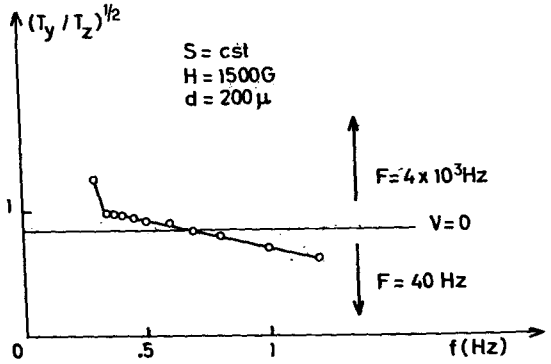

Fig. 14. — This curve is an extension below the axis V = 0 of the usual instability one (*Fig.* 5, 7, 12). In addition to the data points for a high frequency field obtained above the line V = 0, points below this line correspond to the effect of an increasing low frequency one (T_y/T_z decreases as E_l increases). No discontinuity of slope is found around the point V = 0. F is the field frequency, *f* the shear frequency.

On Figure 14 a threshold curve, measured at constant shear, is given in terms of $(T_y/T_z)^{1/2}$. The T_y/T_z values have been determined by the method described above. If no electric field is applied, we have $T_y/T_z = 0.82$.

We note that the cusp shape curve which we had only been able up to now to draw for values of T_y/T_z larger than this limit value by using a high frequency field E_h extends continuously, with no discontinuity of slope, for smaller ratios of T_y/T_z.

It is possible to estimate both the n_y and n_z variation using the laser beam diffraction technique if the beam is oblique with respect to the shear flow cell and is in the *yz* plane. In a Y mode both alternations will give different diffraction images as the angle between **n** and the beam will be different.

Let us consider the time dependence of n_z and n_y during a period of the shear. We have investigated the effect of the increase of the T_z/T_y

ratio on the time variation of n_z and n_y by applying a low frequency electric field E_l. (In principle, with a high frequency electric field it should be possible to do a complementary study, i. e. to decrease T_z/T_y. However, due to the first-order like character of the Z-mode threshold, one cannot study small distortions in this last case.)

When T_z/T_y is increased, two effect are expected:

(*a*) the fluctuation of n_z during one period becomes smaller;

(*b*) n_y/n_z decreases and tends to zero as $T_z \to \infty$ (i. e. as the applied voltage approaches V_c).

The effect (*a*) can be studied by using a normal incidence laser beam. We have indeed observed that if we increase the electric field E_l the amplitude of the variation of the intensity of a diffraction spot, which characterizes the time variation of n_z, decreases. (The experiment was done at the same distance from threshold for the different values of E_l.)

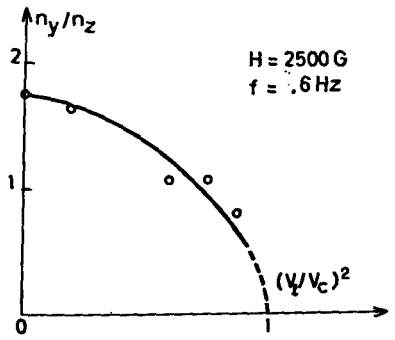

Fig. 15. — By using an oblique incidence beam one can estimate the absolute value of the ratio (n_y/n_z) where n_y and n_z represent the maximum distortions obtained at the end of each half period of a square wave shear. The low frequency voltage applied across the cell V_l is measured with respect to the Williams threshold V_c.

In order to measure n_y/n_z we use an oblique laser beam (which probes differently the n_y and $-n_y$ distortions in the two half periods). The result of a measurement discussed in reference [13] is given on Figure 15. The ratio n_y/n_z corresponds to the times of maximum distortion. We see that n_y/n_z decreases as V_l increases. In the limit of the Williams instability in the absence of a shear, with $V_l/V_c = 1$, we indeed expect that only the n_z distortion will be present ($n_y = 0$).

5. Conclusion

This work has given a rather extensive description both theoretically and experimentally of the continuous and *ac* plane shear flow instabilities in nematic MBBA, extending the studies done in previous works in Orsay (I, II) and by Leslie [4]. The H and R modes obtained in a continuous flow seem to be well understood and quantitatively well described now. We feel that we have enriched the description of the alternating flow: by providing some analytical solutions and numerical ones in the theoretical part; by introducing the notion of minimum displacement applicable to accoustical shear waves; by showing the small influence of the nature ($\sim$ or $\square$) of the alternating flow; by studying the role of a low frequency electric field. However, the description of the alternating mode even near threshold (in particular for the Z mode) s not completely satisfactory.

A very systematic approach has not been done due to the number of parameters involved in the problems and should be done on some simple modes with very well characterized materials where preferably most viscoelastic coefficients should be obtained within the same experiment.

Acknowledgments

We wisk to thank F. M. Leslie for many discussions on these and related subjects. We have benefited of exchanges with I. Jonathan on the properties of phase gratings.

REFERENCES

[1] PIERANSKI P. and GUYON E., *Instability of Certain Shear Flows in Nematic Liquids* (*Phys. Rev.*, Vol. A 9, 1974, pp. 404-417).

[2] PIERANSKI P. and GUYON E., *Shear Flow Induced Transition in Nematics* (*Sol. St. Comm.*, Vol. 13, 1973, pp. 435-437).

[3] MANNEVILLE P. and DUBOIS-VIOLETTE E., *Shear Flow Instability in Nematic Liquids: Theory of Steady Simple Shear Flows* (*J. Phys.*, Vol. 37, 1976, pp. 285-296).

[4] LESLIE F. M., *An Analysis of a Flow Instability in Nematic Liquid Crystals* (*J. Phys.*, Vol. D 9, 1976, pp. 925-937).

[5] JANOSSY I., PIERANSKI P. and GUYON E., *Poiseuille Flow in Nematics: Experimental Study of the Instabilities* (*J. Phys.*, Vol. 37, 1976, pp. 1105-1113).

[6] MANNEVILLE P. and DUBOIS-VIOLETTE E., *Steady Poiseuille Flow in Nematics: Theory of the Uniform Instability* (*J. Phys.*, Vol. 37, 1976, pp. 1115-1124).

[7] MANNEVILLE P. and DUBOIS-VIOLETTE E. (to be published).

[8] CLADIS P. E. and TORZA S., *Flow Instabilities in Couette Flow in Nematic Liquid Crystals* [Presented at *I.C.C.S. Symposium*, San Juan, Puerto Rico, 1976 (to be published by Academic Press)].

[9] PIERANSKI P. and GUYON E., *Cylindrical Couette Flow Instabilities in Nematic Liquid Crystals* (*Adv. in Chem. Phys.*, Vol. 32, 1975, pp. 151-161).

[10] CAROLL T. O., *Liquid Crystals Diffraction Grating* (*J. Appl. Phys.*, Vol. 43, 1972, pp. 767-770).

[11] KASHNOW R. A. and BIGCLOW J. E., *Diffraction from a Liquid Crystal Phase Grating* (*Appl. Opt.*, Vol. 12, 1973, pp. 2302-2304).

[12] GALERNE Y., *Étude de l'instabilité électrohydrodynamique de régime diélectrique dans un cristal liquide nématique* (*Thèse de 3e cycle*, Orsay, 1973).

[13] GUYON E., JANOSSY I., JONATHAN I. and PIERANSKI P., *Optical Study of a Shear Flow Induced Convective Instability* (to be published).

[14] DUBOIS-VIOLETTE E., de GENNES P. G. and PARODI O., *Hydrodynamic Instabilities of Nematic Liquid Crystals under ac Electric Fields* (*J. de Phys.*, Vol. 32, 1971, pp. 305-317).

[15] GÄHWILLER Ch., *Direct Determination of the Five Independent Viscosity Coefficients of Nematic Liquid Crystals* (*Mol. Cryst. and Liq. Cryst.*, Vol. 20, 1973, pp. 301-318).

[16] PIERANSKI P. and GUYON E., *Shear Flow Instabilities in Nematic CBOOA* (*Comm. on Phys.*, Vol. 1, 1976, pp. 45-49).

[17] MANNEVILLE P. (to be published).

[18] ERICKSEN F. M., *A Boundary-Layer Effect in Viscometry of Liquid Crystals* (*Trans. Soc. Rheol.*, Vol. 13, No. 1, 1969, pp. 9-15).

[19] DUBOIS-VIOLETTE E., DURAND D., GUYON E., MANNEVILLE P. and PIERANSKI P., *Instabilities in Nematic Liquid Crystals* (to be published in a supplement of *Solid State Physics*).

[20] DUBOIS-VIOLETTE E., *Theory of Instabilities of Nematics under A.C. Electric Fields: Special Effects near the cut-off Frequency* (*J. de Phys.*, Vol.3 3, 1972, pp. 95-100).

[21] BUSSE F. M., *Non Stationarity Finite Amplitude Convection* (*J. Fl. Mech.*, Vol. 28, 1967, pp. 323-329).

[22] MARTINOTY P. and CANDAU S., *Determination of Viscosity Coefficients of a Nematic Liquid Crystal Using a Shear Waves Reflectance Technique* (*Mol. Cryst. and Liq. Cryst.*, Vol. 14, 1971, pp. 243-271).

[23] SCUDIERI F., *High Frequency Shear Instability in Nematic Liquid Crystals* (*Appl. Phys. Lett.*, Vol. 29, 1976, pp. 398-400).

(Manuscrit reçu le 7 mars 1977.)